Chapter 7

Direct-Contact Heat Exchanger

Hua Wang, Qingtai Xiao and Jianxin Xu

Additional information is available at the end of the chapter

http://dx.doi.org/10.5772/66630

Abstract

Direct-contact heat transfer involves the exchange of heat between two immiscible fluids by bringing them into contact at different temperatures. There are two basic bubbling regimes in direct-contact heat exchanger: homogeneous and heterogeneous. Industrially, however, the homogeneous bubbling regime is less likely to prevail, owing to the high gas flow rates employed. The mixture homogeneity and the non-homogeneity of the mixture can be characterized by the Betti numbers and the mixing time can be estimated relying on image analysis and statistics in a direct-contact heat exchanger. To accurately investigate the space-time features of the mixing process in a direct contact heat exchanger, the uniformity coefficient method based on discrepancy theory for assessing the mixing time of bubbles behind the viewing windows is effective. Hence, the complexity of the bubble swarm patterns can be reduced and their mechanisms clarified, and the heat transfer performance in a direct-contact heat exchanger can be elucidated.

Keywords: direct-contact heat transfer, flow pattern, Betti numbers, discrepancy, mixing uniformity

1. Introduction

1.1. Direct-contact heat exchanger

Direct transfer involves two immiscible fluids under different temperatures in contact for heat exchange [1]. Compared with the traditional direct-contact heat exchanger, heat transfer means has more advantages due to a more simple design, low temperature driving force and higher heat transfer efficiency [2, 3]. Direct-contact heat exchangers (DCHEs) make use of gas-liquid phase change heat exchanger within the working fluid. That is to say, DCHEs put to use heat transfer between two kinds of fluid in the absence of a partition. A direct contact heat exchanger can be used for seawater desalination, heat recovery, ocean thermal energy conversion, thermal energy storage systems, etc.[4, 5]. In addition, DCHEs have been applied

to give a good solution in harnessing the solar energy [6] and provide a better understanding of ice formation, growth and detachment from the droplets producing ice slurry [7].

1.2. Mixing efficiency assessment

Mixing plays a fundamental role in many industrial applications, such as chemical engineering, metallurgical process, printing process, medical and bio-medical industries, and has a decisive impact on the overall performance of reaction processes. The purpose of mixing is to obtain a homogeneous mixture; however, many researchers have pointed out that the local mixing and the flow pattern has significant effects on the properties of the final products [8]. There is an increased want for measuring and comparing mixing performance. An efficient evaluation of mixing effects is required in those various fields, but as a result of its intricacy, theoretical methods are very limited. Monitoring or measuring the mixing appropriately is of much concern from the practical point of view and for the confirmation of theoretical models as much [9]. The existence of a second phase that makes the continuous phase flow and mixing process more complicated, especially for a direct contact with the boiling heat transfer process. The boiling heat transfer process, in which mixing efficiency assessment is common, is one of the most efficient kinds of heat transfer processes widely used in numerous engineering systems. Hence, the work of characterizing the homogeneous bubbling regimes in a DCHE is one of the most useful and instructive topics in DCHE.

1.3. Bubbling regimes

There are two basic types of bubbling regimes in DCHE: homogeneous and heterogeneous. In the homogeneous bubbling regime, there are few diversifications in the size of the bubbles, and breakage and coalescence phenomena are inappreciable [10–12]. Industrially, nevertheless, the homogeneous bubbling regime is not likely to prevail, thanks to the high gas flow rates used. This is good for the heterogeneous bubbling regime, characterized by a widespread of bubble sizes and crucial frequencies of breakage and coalescence [13]. For an air-water system, Ribeiro and Lage [13] employed transient experimental measuring of the temperature of the liquid, bubbling height, evaporation rate, gas volume fraction and bubble size distributions in a direct-contact evaporator for four surface gas velocities including operation in both homogeneous and heterogeneous bubbling regimes. Ribeiro et al. [14] also analysed the photographs of homogeneous and heterogeneous bubbling regimes using different liquids in a DCHE handling with a perforated-plate sparger. Le Coënt et al. [15] studied the compounding of two staves and a viscous liquid in a classical reactor. He found that there was an alleged “pseudo-homogeneous” state before it was mixed completely homogeneously. In reality, a pseudo-homogeneity was achieved much more quickly (<40 s), but subsequent images revealed that polymers still remained in the reactor. The time of the pseudo-homogeneous state begins is called the pseudo-homogeneous time. In our DCHE, we found that there was a comparatively stable state in the completely heterogeneous bubbling regimes also. Consequently, we defined this completely stable state as pseudo-homogeneous. Peyghambarzadeh et al. [16] found that bubble growth was a considerably complicated process, and detecting distinguishable bubbles was scarcely possible at high heat fluxes, while in this experiment, we have captured the rough sketch of bubbles.

1.4. Image analysis

A literature survey showed that image analysis has been used in transparent laboratory vessels to circumvent the drawback of subjectivity of measurement interpretation. Fortunately, the image processing technology has been widely used for feature extraction in medical and chemical industries. Thus, just that technology of image intensification, these bubble images can be computed with the following methods. Bubble growth is severely a function of flow of heat and liquid flow rate [16]. If the flow rate is lower, larger bubbles are observed at constant heat fluxes. This may be due to the fact that the growth of bubbles weakens with the time which is necessary at the velocity of flow is higher. Hence, the bubbles are smaller than those observed at higher high velocity. Similarly, according to the results of Ref. [16], the effect of heat flux is more meaningful than that of flow velocity. Many small bubbles are created on the heat transfer surface, inventing high turbulence flow at high heat fluxes. Consequently, heterogeneous and pseudo-homogeneous bubbling regimes are necessary and worth learning in a DCHE. At the meantime, it is one of the most challenging tasks of direct-contact heat transfer. The current commonly used method is to do with image processing techniques to acquire the features of bubbling regimes.

1.5. Betti numbers

In 1995, Hyde et al. [17] recommended the topological invariant features the topology penetration structure complexity, in the number of micro-structure processing is one of the two material phases. From the perspective of theory, Betti numbers are the number of handles a special case of a topological invariants in a micro-structure [18]. Algebraic topology provides measurable information on complex objects, and Betti numbers are rough measures of this information. Gameiro et al. [18] came up with a method using the Betti numbers to describe the geometry of the fine-grained and snake-like micro-structures created in the process of spinodal decomposition. The zeroth Betti numbers β_0 figure the number of connected components (pieces) in the space Ω. More accurately, if $\beta_0 = k$, then Ω has exactly k components. The first Betti numbers β_1 state a measure of the number of tunnel structure. In a two-dimensional field, tunnels are decreased to loops. It is a remarkable fact that the size and the shape of the component and the loops and do not affect the number of Betti numbers. Friedrich [19] proposed the same chemical group which used the structure descriptors to distinguish un-related chemical group of chondrite and the application of Betti numbers to research the difference in rock chondrite meteorites. A multiphase mixture usually shows a macroscopic homogeneity consisting scattered fine pieces. With an increase in dispersity of the pieces, the homogeneity of the mixture was increased. In the cracks of the pieces are the blowholes, and a polymerization of blowholes gets an aggregation. The more frequently the pores appear, the more likely agglomeration is to occur at the surface. Moreover, increase in the number of pores showed that the heterogeneity of the mixture was mixed more evenly.

In our previous work, using the Betti numbers for gas-liquid-solid three-phase mixing effects of molten salt system based on the reaction of CH_4 + ZnO were characterized. Nitrogen was used to imitate the gas phase (CH_4) and mainly mixing effect in the sink. The zeroth Betti numbers were used to measure the number of pieces in the patterns, bring about beneficial

parameter to describe the mixture homogeneity, which was the number of masters in the micro-structure occupied by one of the two phases. The first Betti numbers were introduced to describe the mixing heterogeneity of mixture. Because we only quantified the solid-liquid mixed flow pattern, the mixture of nitrogen bubble will disappear after image binarization.

1.6. Heat transfer performance

It must be pointed out that Gulawani et al. [20] studied and founded that the turbulent flow pattern in a gas-liquid interface heat transfer coefficient and the immersed surface has a significant impact. Under Gulawani et al. [20, 21] inspiration and guidance, our work is mainly described the flow pattern characteristics of bubbles under the effect of heat transfer in the DCHE. Dahikar et al. [22] and Tayler et al. [23] used the Betti numbers to represent the heterogeneous and pseudo-homogeneous of bubbles. In addition, the relationship between the Betti numbers and the heat transfer coefficient has been obtained in a DCHE.

1.7. Mixing time.

Both mixing speed and phase transition time in the direct contact boiling heat transfer process are fast. An accurate mixing time is critical to appropriately evaluate computational fluid dynamics models and then enhances equipment understanding and develops scale down models for process characterization and design space definition during late stage process development. In the past few years, many researchers have studied the mixing time and many methods were proposed to measure mixing time. But at present, there is no generally accepted method of measuring mixing time, mainly because of each method is not universal, that is each method has its own limitations, such as conductivity [24], pH [25], the dual indicator system method [26], tracer concentration [27–30], electrical resistance tomography [9], coloration decolouration methods [31], the box counting with erosions method [15] and Betti numbers with image analysis [32]. The limitation of each method has been described in details [31]. In all of the above-mentioned technologies, the Betti numbers are one of the most worthy methods to measure the mixing time and get further information of the mixing process. The Betti numbers can be effectively quantitative mixing time, the development process of mixing and degree of homogeneity. It has been used to characterize the evolution of the bubble group in direct contact with the boiling heat transfer process. But, we found that the Betti number method to be used for mixing time and the different evaluation indexes for mixing time have a similar trend, such as the slope p [15], pH, tracer concentration ct, the percentage of mixed pixels, M(%) [31], and the standard deviation (σG) [26]. These indicators change at the beginning of the mixing and quickly tend to be stable after fluctuations. The mixture of non-uniformity caused these fluctuations. This is the inevitable process of pseudo-homogeneous critical point to determine the influence accurate estimates of mixing time, which has often been overlooked. A literature survey shows that it is mainly used for determining the critical point of mixing time, including the mean value of Betti number (mean method) [32], slope p (slope method) [31], and standard deviation (SD) and the selected threshold [33]. Accurate estimation about the mixing time of work was published less than others, especially the critical point determination impact. The idea of a three-sigma method is inspired and motivated by statistical process control (SPC). According to Woodall [34], SPC can commonly be divided into two

phases. The data of phase I are clean gathered under stable operating conditions, whereas the major of phase II is to detect any changes. The 3σ principle is that if the sample data come from a normal distribution $N(\mu, \sigma^2)$, most of the data (99.73%) will lie within the range [μ-3σ, μ+3σ]. It is imposed to detect outliers in the quality control of samples. If the result is normal, the process of the product specification will lie within the scope μ±3σ of the standard value. Otherwise, the production process is considered to be abnormal. Homoplastically, a changed three-sigma edit test has been successfully used in distributed self-fault diagnosis algorithm for large-scale wireless sensor networks [35]. Our research confirmed that the critical point of the response time ignored may result in significant error in mixing time estimation.

1.8. L_2-star discrepancy

The mixing process in DCHE has been studied by many experiments. Similarly, at present, there is no generally accepted way to measure mixing homogeneity, mainly because each method has its own deficiencies, such as thermal method, conduct metric method, pH method, decolourization methods, Schlieren method, Betti numbers method [36], etc. In all of the above-mentioned technologies, the Betti numbers have been used to characterize the evolution of the heterogeneous and pseudo-homogeneous bubbling regimes. But, with the Betti numbers for characterization of mixing uniformity have a space-time limitation; it may lead to significant errors in the evaluation of mixing uniformity. The key question is how to measure the random bubble swarm of minimum difference of space-time consistency bubble swarm of domain. Fang and Wang putted forward the concept of UD (uniform design) that dispersed experimental points uniformly scattered on the domain. One should choose a set of given all possible designs with amount of minimum difference of laboratories under the design of all possible factors and experimental runs. The above is the basic idea of UD [37]. UD has been widely used since 1980 [38]. Inspired and motivated by Fang [37–39], our main research objects are the study of characteristics of time-space features and analyse the mixing process of numerical simulation and experimental analysis. Uniform design theory and image analysis have been applied to quantitative uniformity of time and space in a DCHE.

1.9. Modified L_2-star discrepancy

Recently, we were vitalized and motivated by Xu et al. [39], by the literature that introduces the relatively not complicated and accurately uniformity coefficient (UC) technology, which is based on image processing technology and the theory of uniform design to determine the mixing time and uniformity in a DCHE. The space-time characteristics can be quantified by means of the uniformity coefficient method, which based on L_2-star discrepancy (UC-LD) and provides a method of direct measurement about the macro-mixing evolution. With the same Betti number just is aimed to separate the local and global uniform [40]. Whereas, the nature of the UC such as rotation invariance has not been explored and it has a lot dependence of calculating the initial conditions of UC, namely UC-LD. Clearly, the L_2-star discrepancy is much easier to calculate numerically according to Heinrich [41]. Unfortunately, the L_2-star discrepancy shows some shortcomings, as pointed out by Hickernell [42]. For instance, it is influenced by all the sub-dimensions of the projection uniformity. In order to overcome these shortcomings, Hickernell studied uniformity of some new measure methods, which are also associated

with the L_2 norm, namely, the centred discrepancy (CD) and the wrap-around discrepancy (WD). The centred discrepancy (CD) and the wrap-around discrepancy (WD) satisfy a Koksma-Hlawka type inequality according to Xu et al. [39]. According to the theory of UC-LD, if the image shows a low CD or WD that can be called homogeneous mixing of a set or bubble swarm pattern, and the use of UC-CD and UC-WD provides at least likely to get a good approximation of mixing bubble swarm of spatial distribution. Additionally, UC-CD and UC-WD exhibit some advantages including rotation invariance, reflection invariance and projection uniformity [39].

1.10. Chapter structure

The chapter is organized as follows. In the next section, experiments and methodology are presented; the results and discussion are presented subsequently; the conclusion is briefly summarized in this section finally. Then the acknowledgements and references are presented in the end.

2. Measurement of mixing uniformity in DCHE

2.1. Experimental

2.1.1. Apparatus

The schematic of the experiment employed in the present research is sketched in **Figure 1** [32]. There are two circulation loops in the test device for this experiment. The first loop, which consists of the DCHE (1), electric heater (2), heat transfer fluid (HTF), pump (7) and connecting inlet and outlet pipelines, is a continuous-phase circulation loop for fluid flow, and the other, which consists of the DCHE (1), centrifugal pump (4), plate condenser (5), centrifugal pump (6) and connecting inlet and outlet pipelines, is a dispersed-phase circulation loop for working medium flow. The temperature control device, gear oil pump (3), regulates the initial temperature difference arising from heat exchange. The frequency control cabinet, gas mass flow-meter (8), regulates the rates of flow of the HTF and working medium. The patterns were imaged by a high-speed shutter video camera, which was placed at the second viewing window. In the bubble evaporation process, we could observe the most active stage of the bubbling regime. HTF and the refrigerant R-245fa (1, 1, 1, 3, 3 pentafluoropropane) were used as the continuous phase and the dispersed phase in all runs, respectively.

2.1.2. Experimental design

The settings of the experimental plan affecting the heat transfer capacity of the tested DCHE are determined through the orthogonal array (OA) experimental design method.

As listed in **Table 1**, design parameters with four factors and three levels were selected to investigate the influence of heat transfer capacity. The $L_9(3^4)$ orthogonal array table was chosen for designing the experiment. The interaction between the design parameters was neglected in the present study. H is the height of HTF in the DCHE, ΔT is the initial heat transfer temperature difference, U_g is the refrigerant flow rate, and U_0 is the flow rate of the HTF.

http://dx.doi.org/10.5772/66630

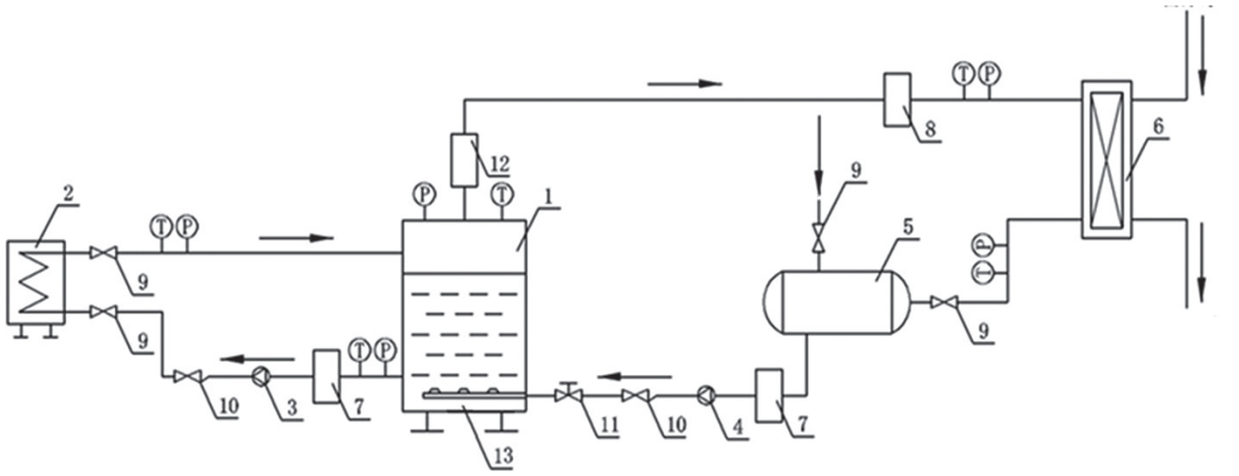

Figure 1. Experimental equipment for direct-contact heat transfer.

Symbol	Design parameter	Unit	Level		
A	H	mm	460	530	600
B	ΔT	K	80	100	120
C	U_g	m^3/s	1×10^{-4}	2×10^{-4}	3×10^{-4}
D	U_0	kg/s	0	0.15	0.3

Table 1. Design parameters and levels.

As shown in **Table 2**, the numbers E_1–E_9 denote different experimental levels according to the orthogonal array table.

2.2. Pattern acquisition and processing

A high-speech video camera was employed to obtain the patterns, and the brand used was PRAKTICA from Germany, with resolution 4 million pixels with no LED light. The images,

Experimental	E_1	E_2	E_3	E_4	E_5	E_6	E_7	E_8	E_9
H(mm)	460	460	460	530	530	530	600	600	600
ΔT(K)	80	100	120	80	100	120	80	100	120
U_g ($\times 10^4 m^3/s$)	1	2	3	2	3	1	3	1	2
U_0 (kg/s)	0	0.15	0.3	0.3	0	0.15	0.15	0.3	0

Table 2. Design experiments according to four factors and three levels orthogonal table.

which were blurred in photographing, can be improved using some image processing techniques. It takes 8 minutes to shoot in each occasion of the orthogonal experiment. Because of difficulties in storing and calculating these images, we choose equal interval sampling from 6000 images, in total, 12,000 images are collected.

Figure 2 is randomly obtained in the present image-processing process. In order to suppress the background of the original image, eliminate noise and enhance the image, gray-scale transformation, top-hat transform is used here. The binaruzation operation was used to calculate the Betti numbers. With a dilation process, an erosion process named as an opening was executed. This process, aiming at removing tiny or isolate points at the finer locations, and smoothing the boundaries of larger points, could not change the size of the image significantly. In contrast, with a dilation erosion process, a dilation process named as an opening was executed. This operation, aiming at filling up tiny pores within the points, connecting nearby points, and smoothing the borders, could not alter the size of the image significantly. The opening is used here to remove small holes representing sile bubbles or small bubble swarms of the binarization images. Since the behavioural characteristics of bubble swarms could not be accurately portrayed by binarized images with noise, an opening operation must be executed to eliminate image noise by the appropriate thresholds selected.

Thus, the white area indicates the bubble swarm, and the black area refers to the continuous phase. As the experimental conditions, the captured image is relatively fuzzy; however, its quality can be improved by using the digital image processing techniques. The resultant image that could be used for the following analysis was identifiable.

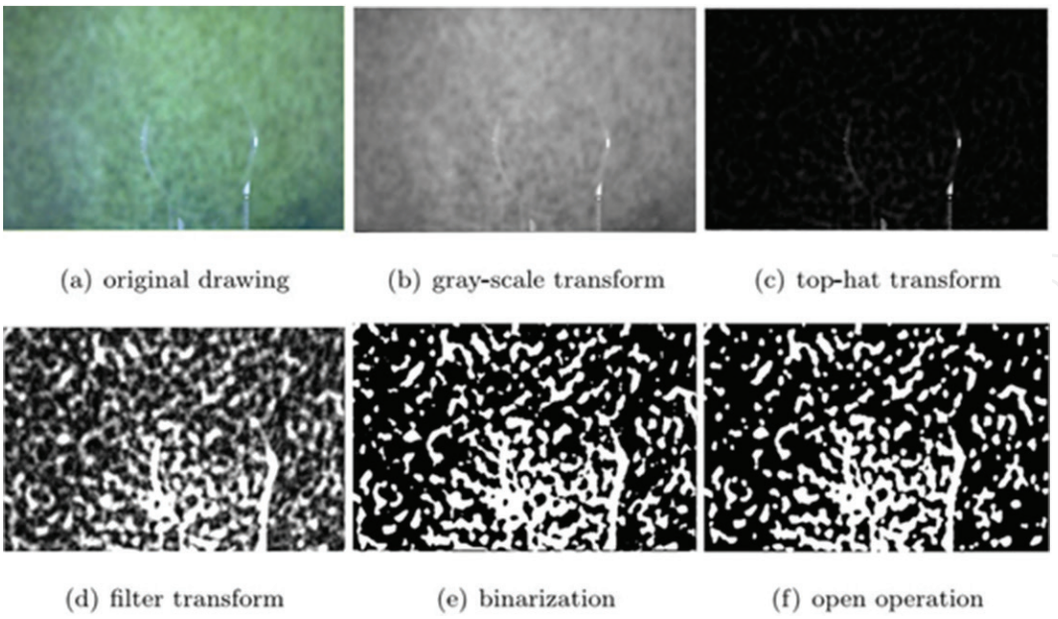

Figure 2. Treatment for one piece of bubble swarm patterns.

2.3. Methodology

2.3.1. Performance evaluation of the DCHE model

Owing to the complexity of the DCHE multiphase structure, heat exchange performance has often been expressed in terms of the volumetric heat transfer coefficient, h_V, which is given by [43]:

$$h_V = \frac{Q}{V \times LMTD} \tag{1}$$

where V is the volume of the continuous phase in the DCHE, and Q is the rate of heat transfer from the continuous phase to the dispersed phase, given by:

$$Q = m\left(h_{do} - h_{di}\right) \tag{2}$$

where m is mass flow-rate of the dispersed phase steam, and h is the enthalpy of the dispersed phase. The *LMTD* in Eq. (1) is the logarithmic mean temperature difference, which is defined as:

$$LMTD = \frac{\left(T_{ci} - T_{do}\right) - \left(T_{co} - T_{di}\right)}{\ln \frac{\left(T_{ci} - T_{do}\right)}{\left(T_{co} - T_{di}\right)}} \tag{3}$$

where T is temperature. In all the equations, the subscript c refers to the continuous phase, d refers to the dispersed phase, i refers to the inlet, and o refers to the outlet.

2.3.2. Computational homology (Betti numbers)

Box-counting with erosions method, which was developed by Le Coënt et al. [15], can be applied to quantify the mixture homogeneity; however, it is not available for quantifying the mixture non-homogeneity. As shown in the experiment, some agglomerates still exist in the vessel after stirring for quite a long time. With computational homology, an original analysis method aiming at getting the quantification of the mixture homogeneity and non-homogeneity was proposed.

As we all know that the zeroth Betti number and the first Betti number have the following information [18, 44]: β_0 equals the number of connected components that make up the space, and β_1 provides a measure of the number of tunnels in the structure. In a two-dimensional domain, tunnels are reduced to loops. Since an image is three-dimensional, it has three Betti numbers: β_0, β_1, and β_2. β_2 measures the number of completely enclosed cavities, such as the interior of a sphere. β_0 indicates the number of pieces, and β_1 represents the number of the holes. In other words, the mixing effect will vary with the number of pieces in the glass vessel. So β_0 and β_1 are used to get such a characterization of the mixture homogeneity and the mixture non-homogeneity, respectively.

β_0, β_1 and their averages $\bar{\beta}_0$, $\bar{\beta}_1$ of the binary images of the patterns can be obtained at different submerged lengths of the lance and flow rates of the gas. Also, we may obtain the value of

time T (time unit: seconds) at which β_0 of the black/white image is equal to $\bar{\beta}_0$. The time T can be employed to obtain the minimum mixing time.

Set

$$\chi^+ := \left\{ t \middle| \beta_0(t) > \bar{\beta}_0, t > T \right\} \quad \chi^- := \left\{ t \middle| \beta_0(t) < \bar{\beta}_0, t > T \right\} \quad A := \frac{1}{2}\left[\frac{1}{m} \sum_{t \in \chi^+} \beta_0(t) - \frac{1}{n} \sum_{t \in \chi^-} \beta_0(t) \right] \quad (4)$$

where $\beta_0(t)$ denotes the zeroth Betti number of the binary image of the pattern, which is captured at the time t, and m, n are the numbers of elements in χ^+, χ^-. A is used to estimate the deviation amplitude of β_0(t) from their average $\bar{\beta}_0$.

In two-dimensional cases, β_0 is the number of connected components, such as black regions. The number of these holes, which is completely enclosed by cubes/pixels, is measured by β_1, and β_1 represents the number of the holes in the domain. One can easily count these white regions. As shown in **Figure 2**, β_0 represents the number of continuous phases, whereas β_1 represents the number of bubble swarms.

The calculation of Betti number is difficult, and the methods are only in their early stages [44]. The free software package CHomP was used to calculate Betti numbers [44, 45]. We could compute β_0 and β_1 of the open operation images of the patterns at different experimental levels using the CHomP software package [45].

Subsequently, we obtained the value of time t (seconds) that can be used to estimate the pseudo-homogeneous time with β_1 representing the average of β_1 of the open operation image after the pseudo-homogeneous process. The bubble sizes were found to be almost the same by inspecting many test images. With the pseudo-homogeneous time, the entire visible area was covered by the bubbles [36]. Just as we all known, combining the evolution of Betti numbers, we can distinguish whether the distribution is uniform or not. In the beginning, the Betti number increases and then rapidly stabilizes after fluctuations.

As **Figure 3** shows, a conversion operation of open operation images was performed. The results showed that a black-and-white conversion directly leads to a switch between the corresponding objects of the zeroth and first Betti numbers [46]. To illustrate, β_0 and β_1 represent the number of the continuous phase in Figure 3a, and the opposite in Figure 3b, respectively. Since it is the white pores that most directly reflect the flow patterns of the bubble swarms, β_1 is still used to characterize the number of bubble swarms.

2.3.3. Three-sigma method

Let X be a normally $N(\mu, \sigma^2)$ distributed random variable. For any $k > 0$, $P\{|X- \mu| < k\sigma\} = 2\Phi\{k\}-1$, where $\Phi\{\cdot\}$ is the distribution function of the standard normal law; whence, in particular, for $k = 3$ it follows that $P\{ \mu-3\sigma < X < \mu+3\sigma\} = 0.9973$. The latter equation means that X can differ from its expectation by a quantity exceeding 3σ on the average in not more than 3 times in a thousand trials [47]. This circumstance is sometimes used by an experimenter in certain problems, by assuming that $\{|X- \mu| > 3\sigma\}$ is practically impossible, and consequently, $\{|X-\mu| < 3\sigma\}$ is practically certain. The probability of exceeding the range of "$\mu \pm 3\sigma$" occurring

http://dx.doi.org/10.5772/66630

twice is 7.29×10^6. Indeed the experimental time series of Betti numbers approximate normal distribution, as shown in **Figure 4** [36].

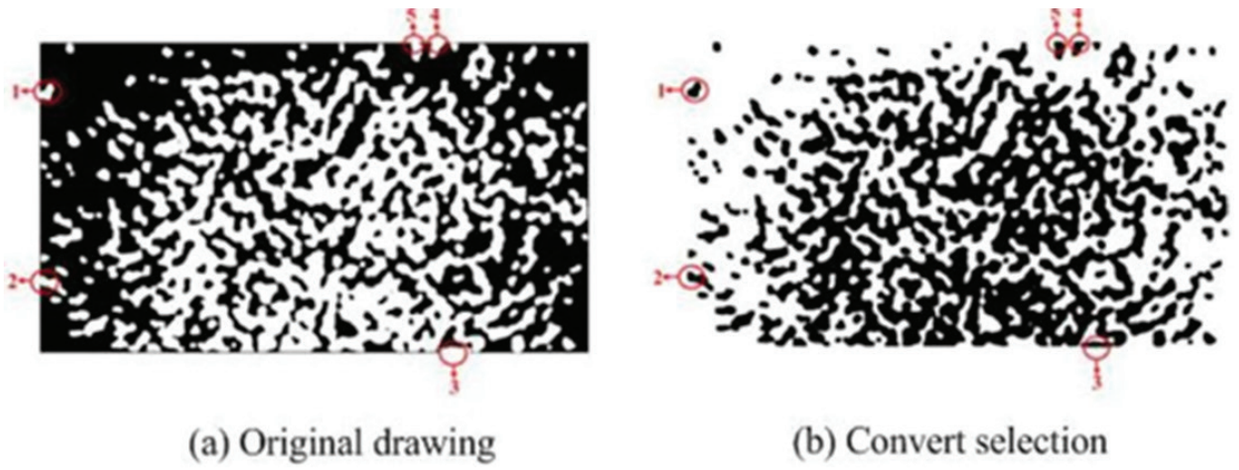

Figure 3. Influence of the boundary on the Betti numbers.

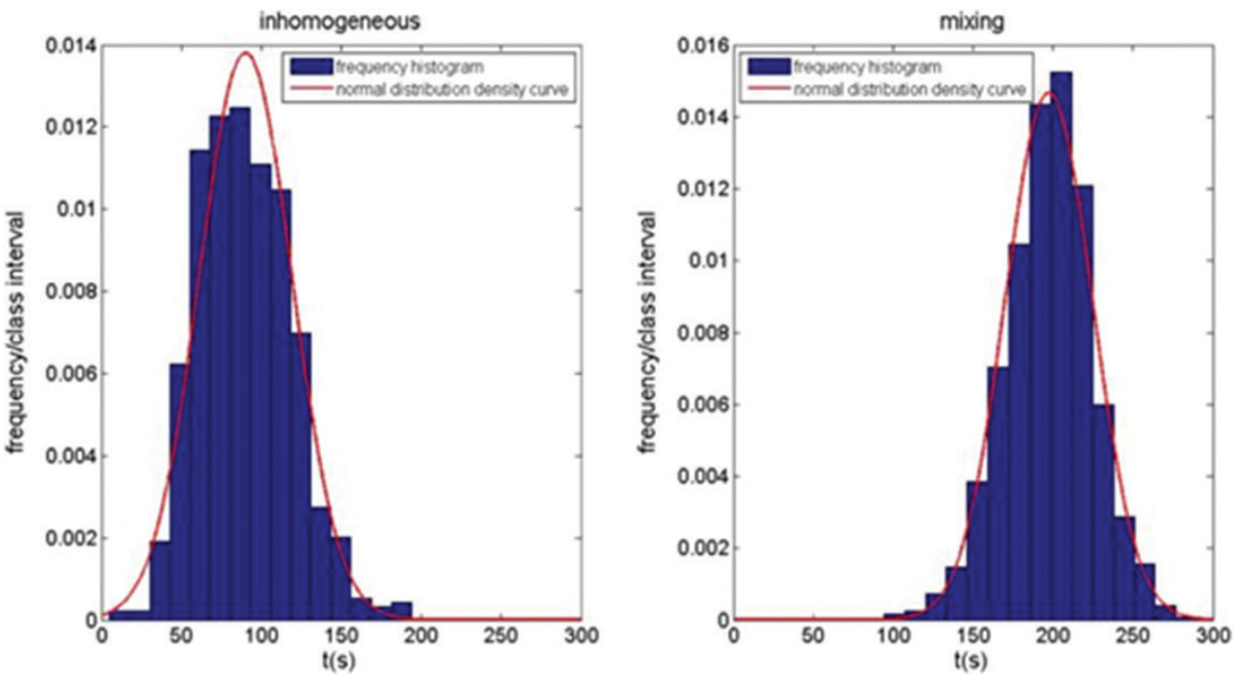

Figure 4. Betti number histogram with a normal distribution fit.

Two consecutive points beyond the limits are viewed as exception criteria.

Step 1: Giving a time point $t_0 > t$, and t is the mixing time, a homogeneous trend was presented during the evolution of Betti number time series of bubble swarm.

Step 2: Calculating the mean t and standard deviation σ of Betti numbers time series after the time t_0.

Step 3: Determining whether an event exceeds the range of "$\mu\pm3\sigma$" occurring twice, as t_0 in reverse order. If so, then the moment is defined as mixing time, t. In order to quantify the macro-mixing efficiency using the Betti numbers, the data of the Betti numbers satisfying approximately normal distribution are collected from mixing homogeneity process, then let μ represents the estimated mean and σ represents the estimated standard deviation, and the mixing time is the time when the critical point exceeds the range of μ-3σ in reverse order twice.

The technique by itself is not limited to transparent tanks. It can be used in conjunction with electrical resistance tomography (ERT), position emission tomography (PET) and magnetic resonance imaging (MRI) [36].

2.3.4. Measures of uniformity

A popular figure of merit is the star discrepancy [48] and its generalization the L_p-star discrepancy. Let $F_u(\boldsymbol{x})=x_1x_2\ldots x_s$ be the uniform distribution function on C^s, where $\boldsymbol{x} = (x_1, x_2, \ldots, x_s)$. Let $F_P(\boldsymbol{x})$ be the empirical distribution function of $P = \{x_1, x_2, \ldots, x_n\}$:

$$F_P(x) = \frac{1}{n}\sum_{i=1}^{n} 1_{[x_i,\infty)}(\mathbf{x}) \tag{5}$$

where $\mathbf{1}_A(\boldsymbol{x})$ is the indicator function. Then the L_p-star discrepancy can be defined as the L_p-norm of difference between uniform and empirical distribution function, and then the L_p discrepancy can be defined as:

$$D_p(P) = \left[\int_{C^s}\left|F_u(\mathbf{x}) - F_p(\mathbf{x})\right|^p dx\right]^{\frac{1}{p}} \tag{6}$$

By taking $p = \infty$, L_∞ discrepancy, which defined as the maximum deviation between these two distributions, is called the star discrepancy [48]. It is probably the most commonly used and can be expressed in another way as follows:

$$D_p^*(P) = \sup_{x\in C^s}\left|F_u(\mathbf{x}) - F_p(\mathbf{x})\right| \tag{7}$$

With the discrepancy criterion in mind, we next discuss how to construct a uniformity coefficient. $\boldsymbol{x}=(x_1, x_2, \ldots, x_s)\in C^s$, $[\mathbf{0}, \boldsymbol{x}] = [0, x_1]\times[0, x_2]\times\ldots\times[0, x_s]$ is the rectangle determined by the origin O and x decided on C^s. $Vol([\mathbf{0}, \boldsymbol{x}])$ denotes the volume of the rectangular solid $[\mathbf{0}, \boldsymbol{x}]$, where $Vol([\mathbf{0}, \boldsymbol{x}])=x_1x_2\ldots x_s=F_u(\boldsymbol{x})$. Let $|\,|$ be the gained number of points in a group. The function of $|P\cap[\mathbf{0}, \boldsymbol{x}]/n|$ represents an empirical distribution, as shown below:

$$F_P(x) = \frac{1}{n}\sum_{i=1}^{n} 1_{[x_i,\infty)}(x) = \frac{|P\cap[\mathbf{0}, \mathbf{x}]|}{n} \tag{8}$$

Definition 2.1. The local discrepancy function is

$$dis\,c^*(x) = F_u(x) - F_P(x) = Vol([\mathbf{0}, \mathbf{x}]) - \frac{|P\cap[\mathbf{0}, \mathbf{x}]|}{n} \tag{9}$$

The difference between theory and empirical distribution can be used to measure the local discrepancy function with a rectangle $[\mathbf{0}, \boldsymbol{x}]$. It can be expressed in another way as follows:

http://dx.doi.org/10.5772/66630

$$dis\, c_i(s,t) = \frac{vo\, l_i(s,t)}{vo\, l_i(\cdot,t)} - \frac{ho\, l_i(s,t)}{ho\, l_i(\cdot,t)} \tag{10}$$

where i denotes the four corners of an image, $i = 1, 2, 3, 4$, vol denotes the volume of the rectangular solid, hol is the number of bubbles.

Definition 2.2. The mean absolute discrepancy is often defined as follows:

$$MAD(s,t) = \frac{1}{4}\sum_{i=1}^{4}\left|dis\, c_i(s,t)\right| \tag{11}$$

In **Figure 5**, the influence of iteration steps on the measurement is not pronounced. The MAD (mean absolute discrepancy) is conducted by the four corners of an image.

Definition 2.3. Uniformity coefficient (UC) at time t is often defined by

$$UC(t) = 1 - Median\{MAD(s,t)\} \tag{12}$$

$$U\,C_1(t) = 1 - \sqrt{\frac{1}{S}\sum_{s=1}^{S} MAD(s,t)} \tag{13}$$

In every case, the degree of mixing uniform could be detected successfully by the uniformity coefficient method (**Figure 6**). After certain processing, the value range of UC is usually [0, 1]. We also denote that the measurement is not pronouncedly affected by the iterative steps.

In **Figure 7**, when the pixels sizes are reduced from 16:9 to 4:3, the influence of homogenization curve by the uniformity coefficient method is not reduced [40]. However, the trend of homogenization curve by Betti numbers method becomes unclear.

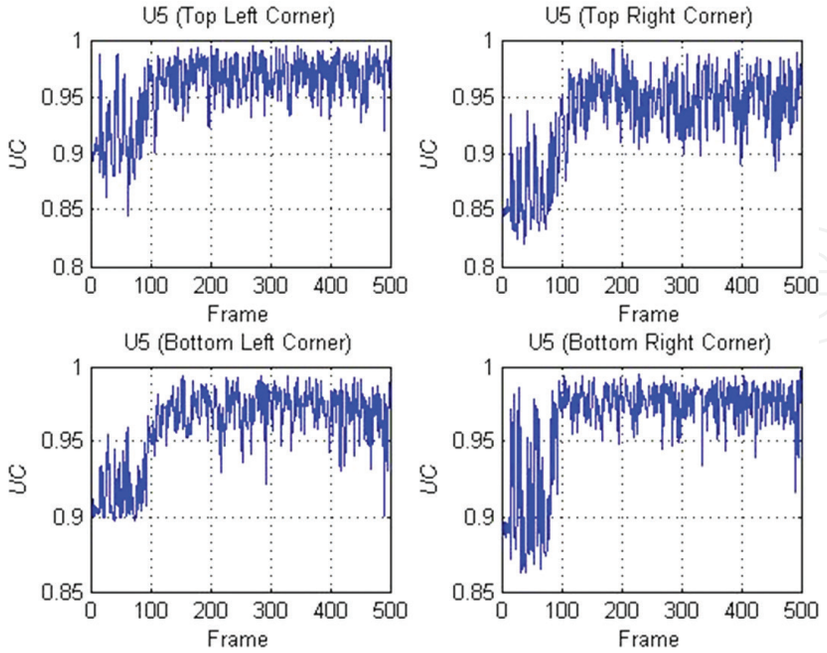

Figure 5. Effect of initial positions on uniformity coefficient.

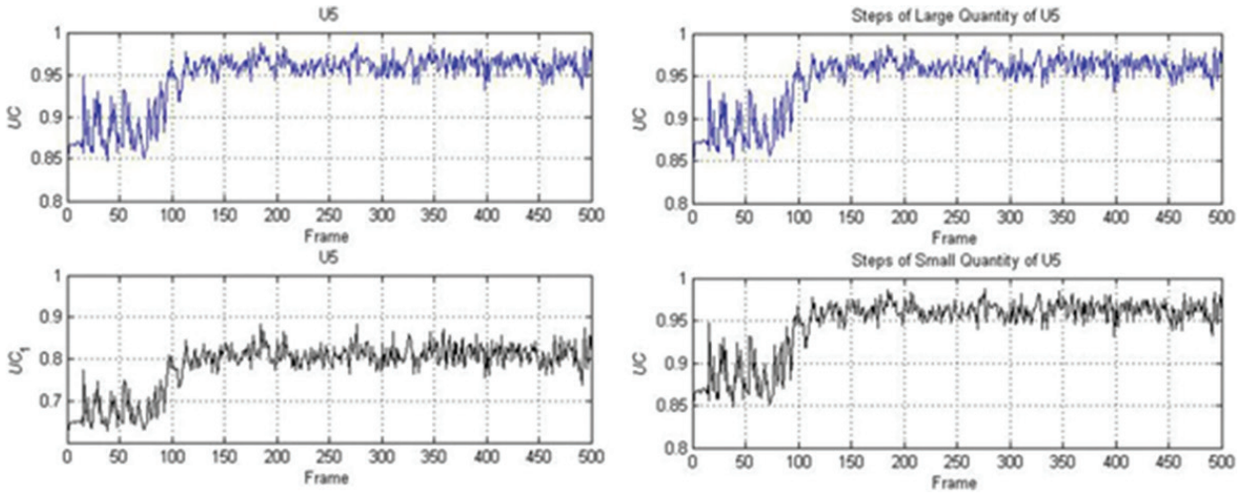

Figure 6. Effect of expressions (left) and iteration steps (right) on uniformity coefficient.

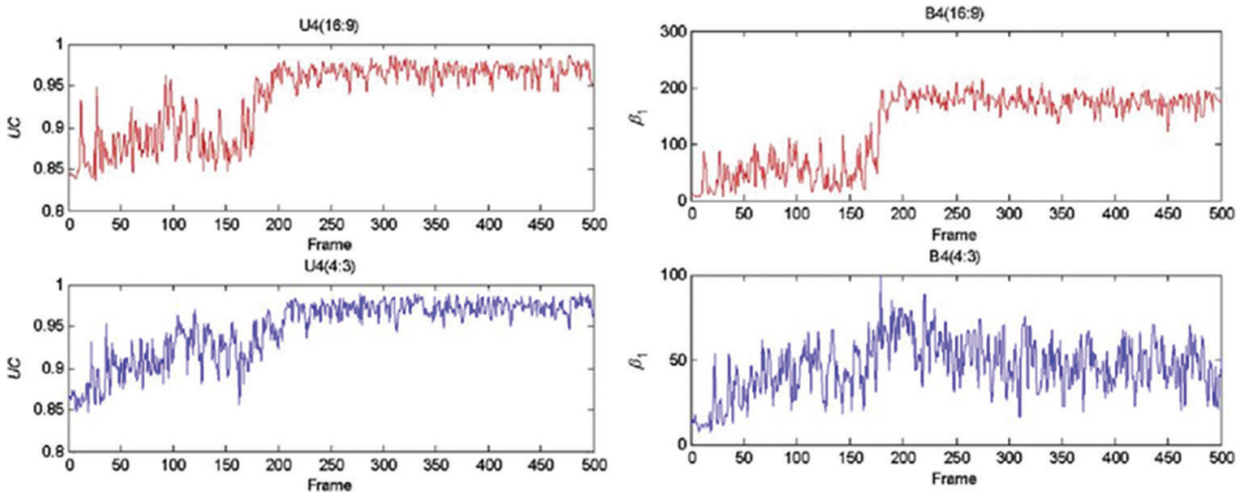

Figure 7. Effect of different pixels (16:9 and 4:3) on uniformity coefficient.

The evolution of the UC and Betti numbers of binary images at different image sizes was clearly shown in **Figure 7**.

Quasi-Monte Carlo method is the most commonly used measure of uniformity in the literature, especially when $p = \infty$ and 2. When $p = 2$, Warnock [49] gave an analytic and simple formula for calculating L_2-star discrepancy as follows:

$$D_2^*(P) = \left\{ \left(\frac{1}{3}\right)^s - \frac{1}{n}\sum_{i=1}^{n}\prod_{j=1}^{s}\frac{1-x_{ij}^2}{2} + \frac{1}{n^2}\sum_{i,l=1}^{n}\prod_{j=1}^{s}\left[1-\max\left(x_{ij}, x_{lj}\right)\right] \right\}^{\frac{1}{2}} \tag{14}$$

where $x_k=(x_{k1}, x_{k2}, \ldots, x_{ks})$. Unfortunately, the L_2-star discrepancy exhibits some limitations, as pointed out by Heinrich and Hickernell [41, 42]. To overcome these disadvantages, other discrepancies were proposed. From the definition of discrepancy, its formula is calculated as follows if objective function takes the uniform distribution function on X:

$$D(P,K) = \left\{ \int_{X^2} K(x,y)\mathrm{d}F_u(x)\mathrm{d}F_u(y) - \frac{2}{n}\sum_{i=1}^{n}\int_X K(x,y)\mathrm{d}F_u(y) + \frac{1}{n^2}\sum_{i,k=1}^{n} K(x_i,x_k) \right\}^{\frac{1}{2}} \tag{15}$$

According to Fang et al. [50], the reproducing kernel functions are taken, respectively, as follows,

$$K^c(z,t) = 2^{-s}\prod_{j=1}^{s}\left(2 + \left|z_j - \frac{1}{2}\right| + \left|t_j - \frac{1}{2}\right| - \left|z_j - t_j\right|\right) \tag{16}$$

$$K^w(z,t) = \prod_{j=1}^{s}\left(\frac{3}{2} - \left|z_j - t_j\right| + \left|z_j - t_j\right|^2\right) \tag{17}$$

hence, the analytical expressions for centred discrepancy and wrap-around discrepancy are as follows:

$$\begin{aligned}\mathrm{CD}(t) = \Bigg\{ &\left(\frac{13}{12}\right)^s - \frac{2}{n}\sum_{i=1}^{n}\prod_{j=1}^{s}\left(1 + \frac{1}{2}\left|x_{ij} - 0.5\right| - \frac{1}{2}\left|x_{ij} - 0.5\right|^2\right) \\ &+ \frac{1}{n^2}\sum_{i=1}^{n}\sum_{k=1}^{n}\prod_{j=1}^{s}\left(1 + \frac{1}{2}\left|x_{ij} - 0.5\right| + \frac{1}{2}\left|x_{kj} - 0.5\right| - \frac{1}{2}\left|x_{ij} - x_{kj}\right|\right)\Bigg\}^{\frac{1}{2}}\end{aligned} \tag{18}$$

$$\mathrm{WD}(t) = \left\{ -\left(\frac{4}{3}\right)^s + \frac{1}{n}\left(\frac{3}{2}\right)^s + \frac{2}{n^2}\sum_{i=1}^{n-1}\sum_{k=i+1}^{n}\prod_{j=1}^{s}\left(\frac{3}{2} - \left|x_{ij} - x_{kj}\right| + \left|x_{ij} - x_{kj}\right|^2\right)\right\}^{\frac{1}{2}} \tag{19}$$

UC-CD and UC-WD related to time t are defined and denoted by

$$\mathrm{UC-CD}(t) = 1 - \mathrm{CD}(t),\ \mathrm{UC-WD}(t) = 1 - \mathrm{WD}(t) \tag{20}$$

where CD(t) and WD(t) denote the modified discrepancy.

Many bubble patterns are related to time t and one piece of patterns corresponds to one t. For the calculation of UC−CD and UC−WD, using the x-axis and y-axis values of a Cartesian coordinate system to determine the position of bubble swarm is necessary.

Step 1: Transform image matrix to 0–1 matrix.

Step 2: Search the coordinates of one bubble located in top-left and bottom-right corners.

Step 3: Calculate the mean values of rows and columns of the two above coordinates.

In our work, $M = 1280$ and $N = 720$, then readjusting every piece of bubble patterns to unified pixel size of $M \times N$. The image pixel matrix is transformed into coordinate within [0,1]

$$x = \frac{x_0 - 1}{M - 1}, \quad y = \frac{N - y_0}{N - 1} \tag{21}$$

and where x_0 and y_0 denote the column and row of one image matrix, x and y denote the coordinates of horizontal axis and vertical axis in Cartesian coordinate system. Furthermore, in this work, $s = 2$, so (x, y) of one experimental point is equal to (x_{i1}, x_{i2}) of Eqs. (7) and (8).

The origin of coordinates lies in the bottom-left (BL) corner of one piece of pattern. Certainly, other three groups of transformation ways are used to make origin of coordinates locate in bottom-right (BR), top-right (TR) and top-left (TL) coiners' of one piece of patterns, respectively. Detailed formulas as follows,

$$x = \frac{M - x_0}{M - 1} \quad y = \frac{N - y_0}{N - 1} \quad x = \frac{M - x_0}{M - 1} \quad y = \frac{y_0 - 1}{N - 1} \quad x = \frac{x_0 - 1}{M - 1} \quad x = \frac{y_0 - 1}{N - 1}. \tag{22}$$

More interesting, these transform methods are different but corresponding to the coordinates rotate operation for the rectangular plane coordinate system. Hence, we will talk about the rotational invariance and neglect the different transform methods in next section.

2.4. Mixing quantification by Betti numbers

2.4.1. Multiphase mixing quantification

Now this new method is used to study the influence of the flow rate and the submerged length on the degree of the mixing homogeneity and non-homogeneity of solid and liquid. The acquisition system was shown in **Figure 8**. The patterns were gained at the speed of 30 frames per second by a camera taking 10,000 images in each experiment.

Figure 9 shows that an initial image was subtracted from each image.

2.4.2. Characterization of heat transfer process

Figure 10 shows the evolution of β_1 in the open operation images produced in representative experimental cases. β_1 for each pattern is shown as a solid line, and the horizontal dotted line corresponds to the average of β_1 [32]. The vertical dotted line corresponds to the pseudo-homogeneous time t.

Experiments indicate that, in **Figure 11**, volumetric heat transfer coefficient shows good correlation with average Betti number and pseudo-average-time value [32]. An interesting tendency is found in the better cases of L_6 and L_2, in which the larger first Betti numbers averages and

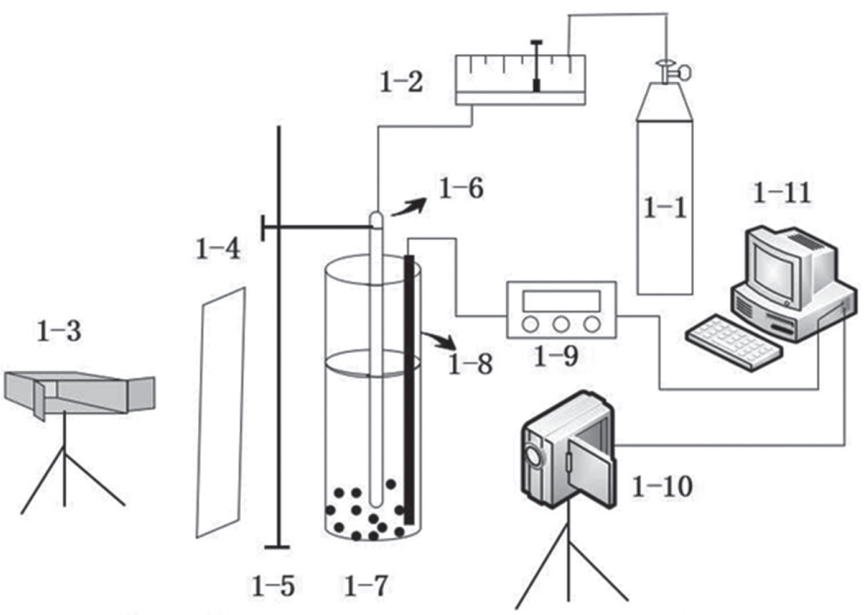

Figure 8. Scheme of experimental equipment.

http://dx.doi.org/10.5772/66630

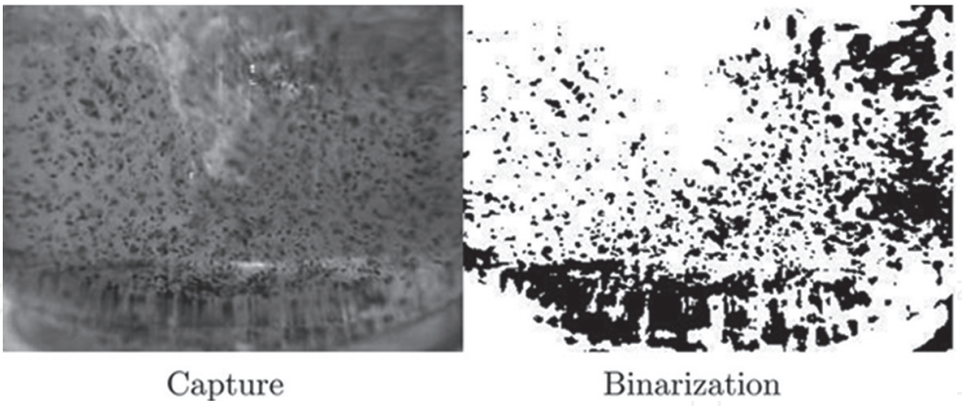

Figure 9. Binarization for one piece of images.

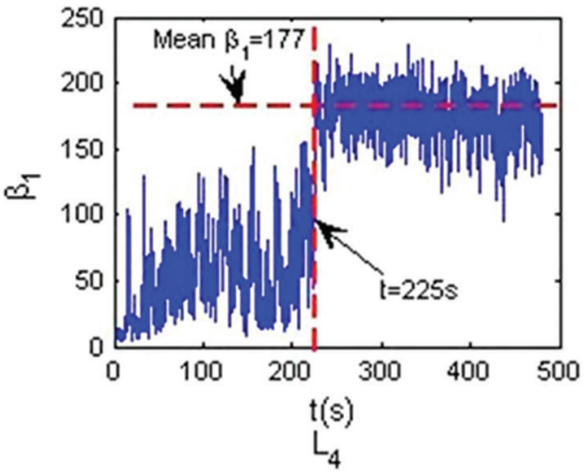

Figure 10. The evolution of Betti numbers at E_4.

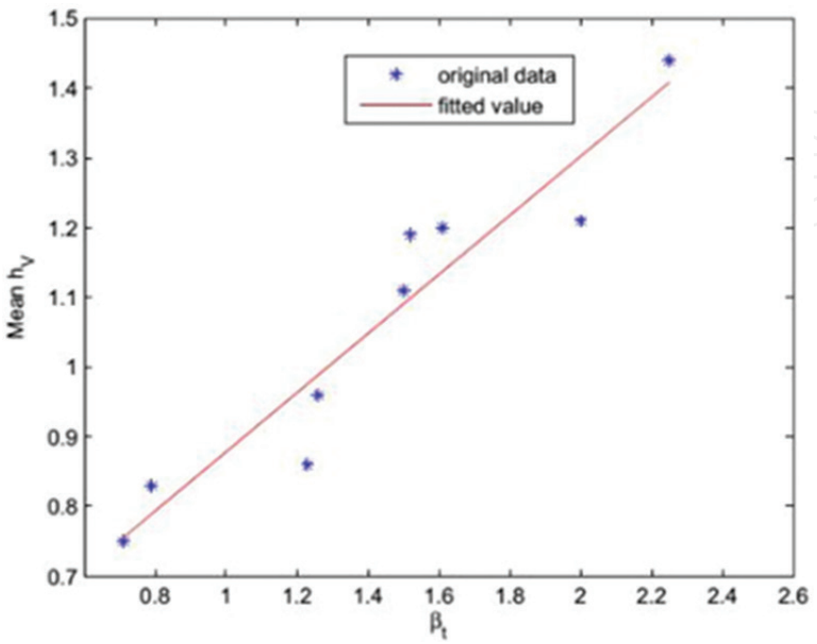

Figure 11. Fitting of β_t and $h^- V$.

shorter pseudo-homogeneous times correspond to a higher volumetric heat transfer coefficient h_V, while L_4 and L_7 are the worse cases. As shown in **Table 3**, t and $\bar{h}_V$ are nearly opposite in all cases except L_5, L_8 and L_9. Therefore, the parameters t and $\bar{\beta}_1$, which can be used to characterize a bubbling flow pattern, are both related to $\bar{h}_V$.

Parameter	E_1	E_2	E_3	E_4	E_5	E_6	E_7	E_8	E_9
T	159	93	120	226	126	92	264	105	145
$\bar{\beta}_1$	197	186	208	177	197	189	187	176	196
β_t	1.26	2	1.23	0.79	1.61	2.25	0.71	1.50	1.52
$\bar{h}_V$	0.96	1.21	0.86	0.83	1.20	1.44	0.75	1.11	1.19

Table 3. The data of the t, $\bar{\beta}_1$, β_t, and $\bar{h}_V$ for the entire orthogonal array table.

Let $\beta_t = \bar{\beta}_1 \cdot t^{-1}$, the tendency of β_t is consistent with that of $\bar{h}_V$. According to our analysis, a linear relation between β_t and $\bar{h}_V$ seems to be the outcome. Let $\bar{h}_V = a \times \beta_t + b$. The least-squares fitting method was used to obtain the parameters a and b between β_t and $\bar{h}_V$. In this work, a = 0.4241, b = 0.4547. The linear relationship is illustrated in **Figure 11**. The correlation coefficient is 0.95. In the end, we constructed a model on the parameters β_t and $\bar{h}_V$, which points out the relationship between the flow pattern of a bubble swarm and the heat transfer performance of a DCHE.

2.4.3. Accurate estimation of mixing time

(1) Mixing time estimations by different methods

Based on the above, β_t has been defined by the Betti number average as well as the mixing time, which is synergistic with $\bar{h}_V$. Correlation degree and correlation coefficient are used to investigate about the bubble swam patterns and heat transfer performance for the mixing time evaluation effectiveness. According to reference [36], the computing results show that the synergy by our 3σ method between β_t and $\bar{h}_V$ is much better than the other methods. In **Figure 12**, the plots show the evolution and determination of mixing time measured by different methods [36].

It is found that the correlation coefficient between $t_{3\sigma}$ and mixing time estimated by these methods is −0.2304 (mean method), 0.9494 (slope method), 0.9265 (SD method) and 0.9731 (3σ method).

In **Table 4**, μ is the mean of Betti number time series after the time t_0. t_{mean} is the mixing time by mean method. t_{slope} is the mixing time by slope method. t_{sd} is the mixing time by SD method. $t_{3\sigma}$ is the mixing time defined by 3σ method. $T_{3\sigma}$ is the inhomogeneous time by 3σ method. δ_t is the difference between $t_{3\sigma}$ and $T_{3\sigma}$. β_{mean} is calculated by mean method, and the others are defined similarly [40]. It can be quantified by time intervals δ_t between inhomogeneous time and mixing time. From the view point of the time interval, the transitional state appears the following forms: sudden change case ($\delta_t = 0$); interval case ($\delta_t > 0$); overlapping case ($\delta_t < 0$).

(2) Simulation experiments

By real data analysis of the Bitti number data, we have compared the proposed method with mean method, slope method and SD method. In order to assess the effectiveness of the new

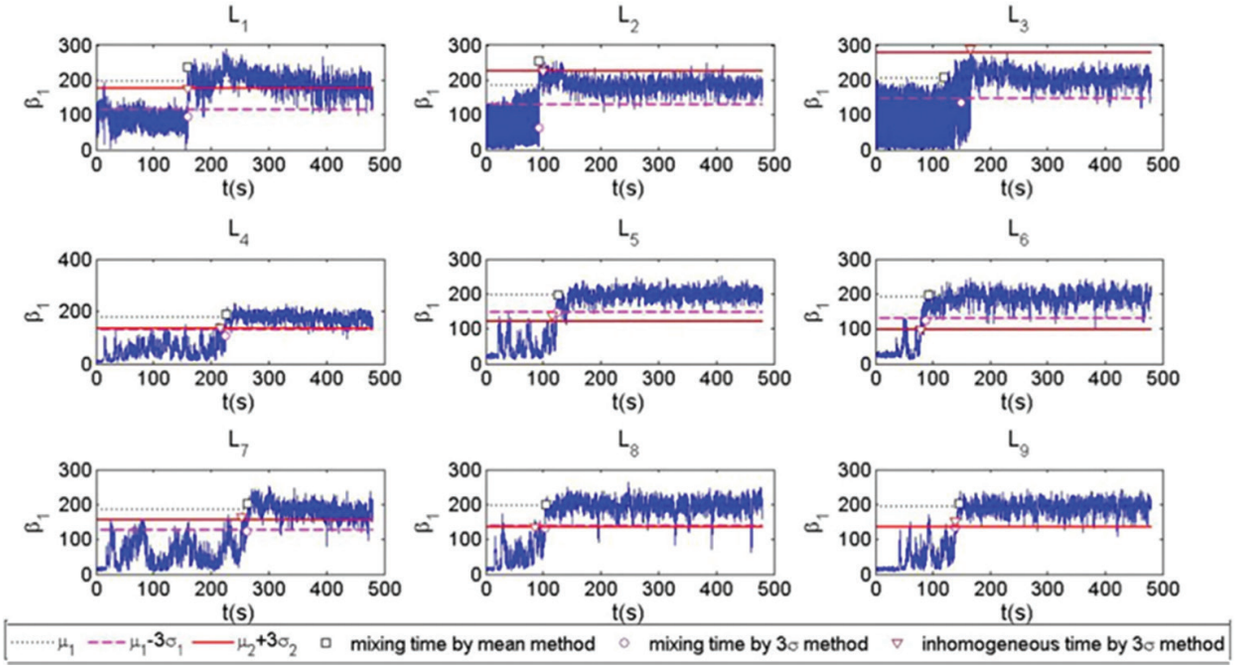

Figure 12. Evolution and determination of mixing time measured by two methods.

method and provide more evidences of good performance of this method, the mean absolute error (MAE) and the mean square error (MSE) are often used.

$$MAE = \frac{1}{n}\sum_{i=1}^{n}\left|t_i - \hat{t}_i\right| \quad MSE = \frac{1}{n}\sum_{i=1}^{n}\left(t_i - \hat{t}_i\right)^2 \tag{23}$$

where t_i is the real mixing time, and $\hat{t}_i$ is the estimate of t_i.

Index	E_1	E_2	E_3	E_4	E_5	E_6	E_7	E_8	E_9
M	197	185	206	177	197	190	186	197	192
t_{mean}	159	93	120	226	126	92	264	105	145
t_{slope}	153	80	112	216	123	83	249	97	137
t_{sd}	135	71	158	177	134	101	232	99	133
$t_{3\sigma}$	159	93	150	225	124	87	262	103	138
$T_{3\sigma}$	159	99	165	215	115	79	252	85	139
δ_t	0	−6	−15	10	9	8	10	18	−1
β_{mean}	1.24	1.99	1.72	0.78	1.56	2.07	0.70	1.88	1.32
β_{slope}	1.29	2.31	1.84	0.82	1.60	2.29	0.75	2.03	1.40
β_{sd}	1.46	2.61	1.30	1.00	1.47	1.88	0.80	1.99	1.44
$\beta_{3\sigma}$	1.24	1.99	1.37	0.79	1.59	2.18	0.71	1.91	1.39

Table 4. Computing results of mixing performance by four methods.

From **Table 5**, we can see that proposed method has a distinct advantage [36]. **Figure 13** shows an example of 1000 simulation results.

Index	Mean method	Slope method	SD method	3σ method
MAE	6.22	6.66	8.07	3.38
MSE	41.78	44.85	101.85	12.11

Table 5. Comparison of computer simulation results by 1000 times.

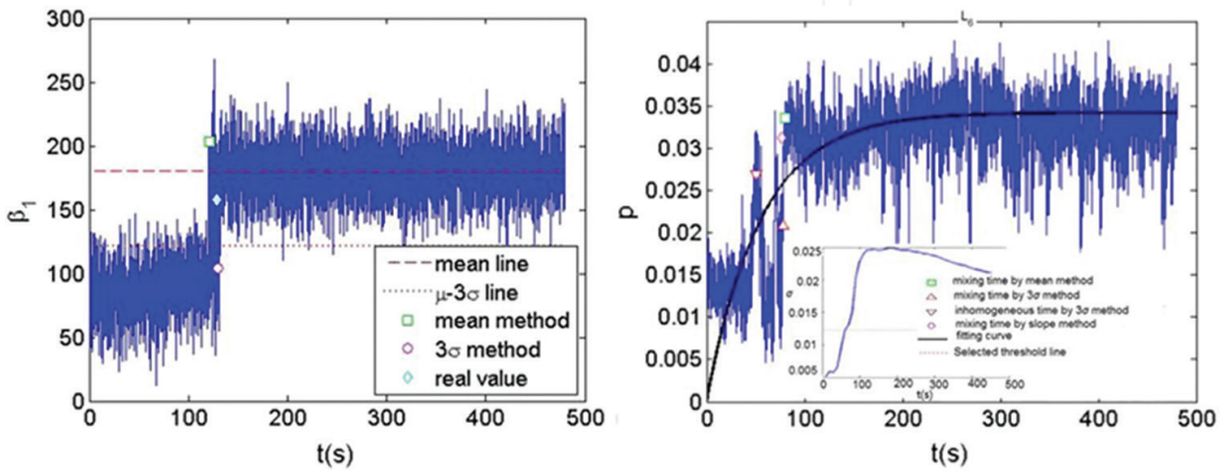

Figure 13. One of these simulation results by 1000 times.

2.5. Measuring bubbles uniformity by discrepancy

2.5.1. Quantifying mixing efficiency using L_2-star discrepancy

(1) Quantification of mixing efficiency

The variation of the uniformity coefficient with frames can be an effective method to determine the critical mixing time and mixing uniform.

In **Figure 14**, quantitative comparisons of the homogenization curve and mixing time predicted by the uniformity coefficient method are conducted with reported experimental data and other predictions by the Betti numbers method.

The comparisons show that good agreements of the mixing time obtained by Betti numbers method and uniformity coefficient method have also been achieved as given in **Table 6** [40].

(2) Recognition of local and global uniformity

Numerical simulations. Generated small sets were used with the same Betti number randomly to assess the performance of the UC implementation for approximating the discrepancy of a given set of points. By checking a large number of experimental images, we found the sizes

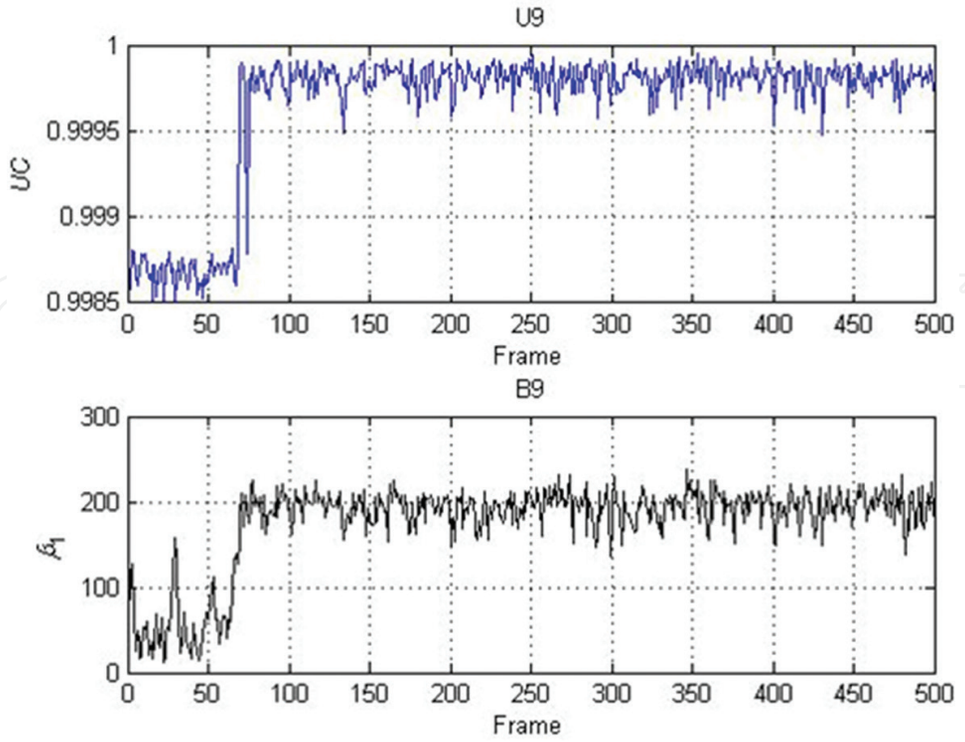

Figure 14. Evolution of mixing efficiency by the uniformity coefficient method (denoted as U9) and Betti numbers method (denoted as B9).

Parameter	E_1	E_2	E_3	E_4	E_5	E_6	E_7	E_8	E_9
t	159	93	120	226	126	92	264	105	145
t^*	151	97	172	224	120	84	259	118	127

Table 6. Computing results of mixing time by the Betti numbers method (t) and uniformity coefficient method (t^*) at the whole orthogonal arrays table.

of the bubbles are nearly the same. Two hundred and thirty-four bubbles have the same small blank area of the radius of the circle. MATLAB software randomly selects the centre. Although 234 bubbles have the same size, they are spread in different places.

These plots of **Figure 15** are got by simulation with 720 lines and 1280 rows. Among them, the simulation 1 (**Figure 15a**) is the corresponding local uniform description, simulation 2 (**Figure 15b**) corresponds to the portrayal of global uniform. The lattice points generate the example of lattice uniform used in the demonstration of the algorithm. Under the guidance of the lattice points method, the simulation 3 (**Figure 15c**) performs for a lattice points set, which has 234 bubbles. It is can be seen that the lattice uniform is most accurate uniformly. One can take set of points or objects, which are generated by these experiments and simulations to check the algorithm.

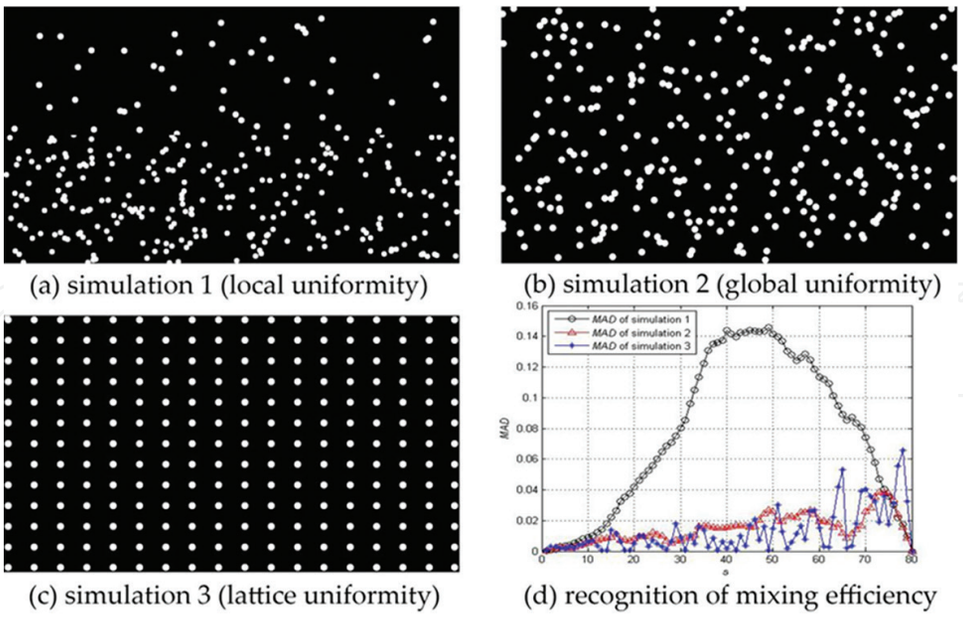

Figure 15. Numerical simulations and MAD evolutions of different mixing efficiency.

Experimental examples. The plots in **Figure 16** are obtained by experiments E_3 and E_6. The experiments are response to the worse and better cases. **Figure 16a–c** shows the difference of mixing uniformity in case 1 of E_6 with $\beta_1 = 160$, whereas **Figure 16e**, **d**, and **f** shows the difference of mixing uniformity in case 2 of E_3 with $\beta_1 = 194$. Comparison results show that the different experimental cases with the same Betti numbers can be identified by the MAD evolutions. The results in **Figure 16** indicate that the uniformity coefficient method might be enough to obtain a good estimation and quantification of multiphase mixing effects.

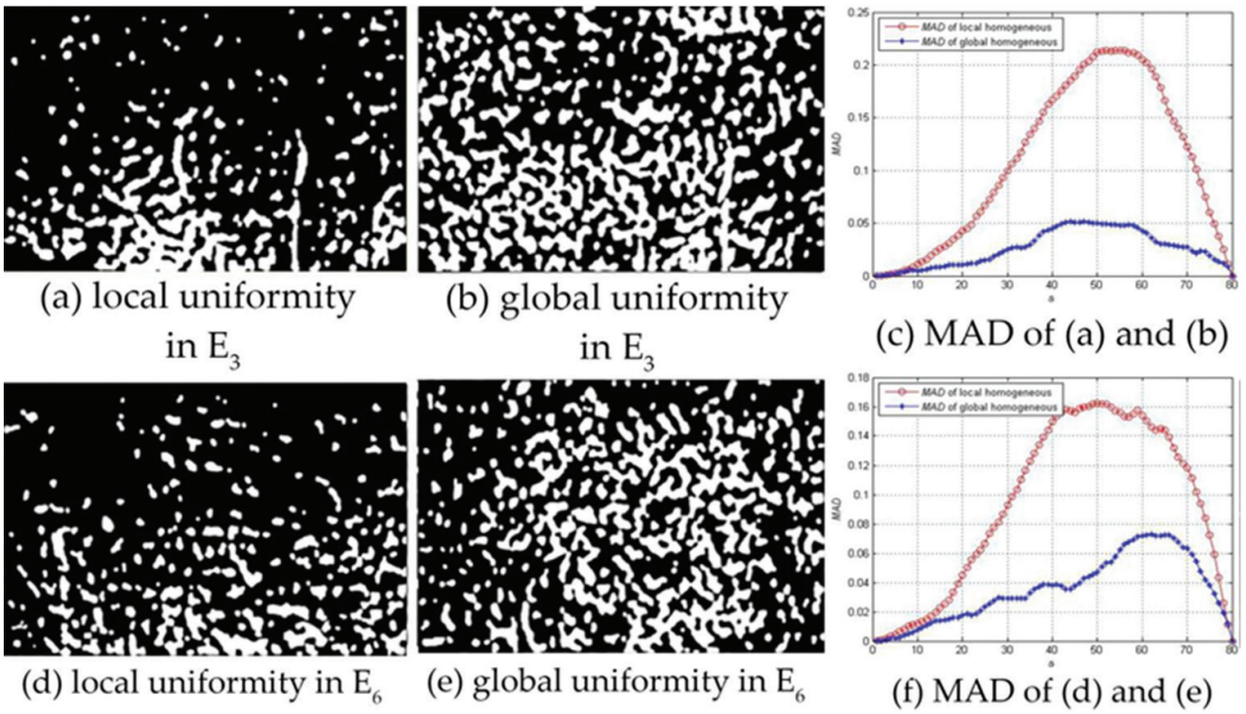

Figure 16. MAD evolutions of different experimental cases with the same Betti numbers.

2.5.2. Modified L_p-star discrepancy for measuring mixing uniformity

(1) Video-frequency image sequence of experimental cases

In **Figure 17**, quantitative comparisons of the homogenization curve utilizing uniformity coefficient with modified discrepancy methods are conducted with reported experimental data and the other method is UC-LD. The variation of the UC-LD and UC-WD versus i can be effectively used to estimate the critical mixing time and mixing uniform because of the similar evolutionary trend and regularity of most experimental cases. Especially here there is a clearly and distinctively different at the early phase of mixing process of experimental case E_2 (see **Figure 17a**), and obvious differences in numerical performance have a deep significant role to assess the mixing efficiency. For another experimental case E_7, UC-CD and UC-WD successfully measured the mixing process from no uniformity to uniformity clearly, just like UC-LD (see **Figure 17b**).

(2) Verification of properties

Suppose coordinates of bubble swarms in **Figure 2** can be denoted as follows,

$$X_p = \begin{pmatrix} x_{11} x_{21} \\ x_{21} x_{22} \\ \vdots \quad \vdots \\ x_{n1} x_{n2} \end{pmatrix} \tag{24}$$

where n is the number of bubble swarms or experimental points noted earlier. With one important note as mentioned above, the first rank elements x_{11}, x_{21},…, x_{n1} of X_P correspond to the x values identified in Eq. (21) the second rank elements x_{12}, x_{22}, …, x_{n2} of X_P correspond to the y values identified in Eq. (21). UC-CD and UC-WD are formulated as the two methods of measures of uniformity. In addition, they are dimensionless, which vary from 0 to 1. And it is hard for it to reach the certain endpoint values.

Invariance to permutation. UC-CD and UC-WD are permanent for disrupted order of the experimental factors or the experimental points. **Table 7** shows verification data about invariance to permutation. Bubbles disordered in **Table 7** means that the operator randomly shuffles

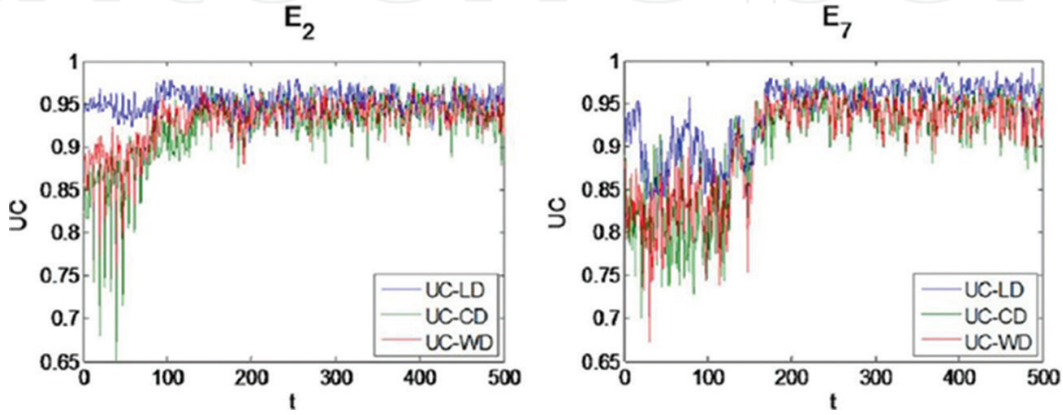

Figure 17. Uniformity coefficients of E_2 and E_7.

rows in Eq. (24). Coordinates disordered in **Table 7** means that the operator randomly shuffles columns in Eq. (24). It is quite clear found that the two parameters identically equal to 0.9751 and 0.9723 individually even though the disorder of rows or ranks happened.

Modified UC	In proper order	Disordered Bubble	Coordinates	Both
UC-CD	0.9289	0.9289	0.9289	0.9289
UC-WD	0.9311	0.9311	0.9311	0.9311

Table 7. The data of verification of invariance to permutation.

Invariance under reflection. In theory, UC-CD(P) and UC-WD(P) are invariant if x_{i1} and x_{i2} are replaced individually by 1-x_{i1} and 1-x_{i2}, $1 \le i \le n$. The data of verification of invariance under reflection are depicted in **Table 8**. More in detail, $x = 1/2$ in **Table 8** means that the operator rotates the origin of coordinates system from bottom-left to bottom-right in a piece of patterns, $y = 1/2$ in **Table 8** means that the operator rotates the origin of coordinates system from bottom-left to top-left in a piece of patterns, $x = 1/2$ and $y = 1/2$ (both) in **Table 8** means that the manipulator spins the origin of coordinates system from bottom-left to top-left. It is obviously found that the two parameters individually equal to 0.9751 and 0.9723 even though the origin of coordinates system is rotated.

Projection uniformity. The projection uniformity over all sub-dimensions can be considered, and UC-CD(P) and UC-WD(P) are also invariant to it in theory. The data of verification of projection uniformity are depicted in **Table 9**. Projected to x-axis in **Table 9** refers to set $x_{i2} = 0$ in Eq. (24), projected to y-axis refers to $x_{i1} = 0$ and projected to origin refers to $x_{i1} = 0$ and $x_{i2} = 0$. It is quite clear that the projection uniformity over all sub-dimensions can be obtained. All this to say the consideration is not insignificant for high-dimensional cases.

Modified UC	No reflected	Reflected		
		x = 1/2	y = 1/2	Both
UC-CD	0.9289	0.9289	0.9289	0.9289
UC-WD	0.9311	0.9311	0.9311	0.9311

Table 8. The data of verification of invariance under reflection.

Modified UC	No projected	$y = 0$	$x = 0$	Projected to origin
UC-CD	0.9289	0.3946	0.3936	0.0554
UC-WD	0.9311	0.5263	0.5253	0.3128

Table 9. The data of verification of projection uniformity.

(3) Time complexity. The time complexity of different methods is shown in **Table 10**. Through experimental comparison, we may draw the conclusion that UC-CD and UC-WD can replace

UC-LD and Betti numbers to some extent. Determination of the position of bubble swarms spends too much time, which leads to make the upper time complicated. But, other progressive technology can change this disadvantage.

Single image	Betti numbers	UC-LD	UC-CD	UC-WD
Reckoning	$\beta_1 = 174$	0.9632	0.9289	0.9311
Running time (s)	3.07	2.61	18.33	18.23

Table 10. The data of time of different methods.

(4) Numerical simulations and experimental examples. In order to assess the performance of UC-CD and UC-WD implementation for approximating the discrepancy of a given set of points, the three sets in **Figure 14** were used. **Table 11** shows that UC-LD of the three simulated images are affected by initial position, but UC-CD and UC-WD not. Comparing the modified UC of **Figure 14b** and c, the absolute difference $|0.9751-0.9657| = 0.0094$ is less than $|0.9623-0.9464| = 0.0159$ since **Figure 14b** and **c** seems to have the same degree of mixing uniformity. So it is concluded that UC-CD may outperform UC-WD and perform more sensitive for practical engineering application in some sense. The data in **Table 11** also show that the difference of mixing uniformity coefficients including UC-LD, UC-CD and UC-WD with the same Betti numbers in **Figure 16a**, b, d and e. Meanwhile, it is noticed that different initial positions are response to different UC-LDs, which bring unreasonable and bias measurement of uniformity in practice. In other words, UC-LD may result in multiple values, but UC-CD and UC-WD do not have this problem. Moreover, the absolute difference of UC-CDs is larger than that of UC-WDs. The comparison result shows that UC-CD performs more sensitive than UC-WD in identifying the different patterns with the same Betti numbers. Those are the major of our presented work in this part.

2.6. Conclusions

1. Because a new technique based on algebraic topology was introduced for quantifying the efficiency of multiphase mixing, the mixture homogeneity and the non-homogeneity

Plots		UC-LD				UC-CD	UC-WD	TL
		BL	BR	TR	Figure 15			(a)
0.9326	0.9033	0.9381	0.9189	0.8052	0.8493	(b)	0.9854	0.9866
0.9854	0.9955	0.9751	0.9623	(c)	0.9925	0.9932	0.9930	0.9925
0.9657	0.9464	Figure 16	(a)	0.8699	0.9077	0.9094	0.9033	0.9102
0.9170	(b)		0.9826	0.9523	0.9823	0.9869	0.9474	0.9436
(d)	0.8686		0.9507	0.8645	0.9056	0.8793	0.9121	(e)
0.9676	0.9794		0.9504	0.9825	0.9429	0.9306		

Table 11. The data of numerical simulations and experimental examples.

of the mixture can be characterized by the Betti numbers for binary images of the patterns. The zeroth Betti numbers β_0 are used to estimate the numbers of pieces in the patterns, leading to a useful parameter to characterize the mixture homogeneity. The first Betti numbers β_1 are introduced to characterize the non-homogeneity of the mixture. This novel method may be applied for studying a variety of multiphase mixing problems in which multiphase components or tracers are visually distinguishable.

2. In a DCHE, Betti number can estimate the number of bubbles assembling in flow patterns and to get the pseudo-homogeneous time. Experimental analysis constructs a simple linear model representing a bubble swarm and the heat transfer performance of a DCHE. In addition, the Betti number average and the pseudo-homogeneous time t define a new index. A better fitting curve about and the volumetric heat transfer coefficient average is received and its correlation coefficient is 0.95. A paradigm is established on the basis of this novel method for the study of flow patterns and heat transfer performance. And the paradigm offers an optional route to study the relationship of flow patterns and heat transfer in other heat transfer processes.

3. A novel method relying on image analysis and statistics was developed to estimate the mixing time accurately in a DCHE. The three sigma method researches the critical point determination of the pseudo-homogeneous process, which satisfies approximately normal distribution and surpasses the range of occurring twice. The mean value method, slope method and standard deviation method make quantitative comparisons of the mixing time. In addition, time intervals between in-homogeneous time and mixing time quantify the quasi-steady state. Neglecting critical point could make substantial errors in mixing time estimation, which is proved.

4. A straightforward method, uniformity coefficient (UC) method based on L_2-star discrepancy (UC-LD), presented for assessing the uniformity and mixing time of bubbles behind the viewing windows in a DCHE is effective. An imaging technique processed in the MATLAB software tracks the evolution of bubbles movement. The local discrepancy of a set of bubbles seems to be helpful to judge the difference between theory and empirical distribution. The UC links to a discrepancy, leading to a useful parameter which expresses the mixture homogeneity and mixing time. A comparison was made between the mixing time and uniformity obtained by UC method and the data obtained by Betti numbers method. Discussing the simulation and experiments conducted between local and global uniform (with the same Betti numbers) and examples are given for illustration. UC method calculates the space-time features of the mixing process successfully. The UC curves can study and compare mixing efficiency of different systems with the novel method, which can generate accurate mixing information and has a well reliability.

5. The properties of UC have been explored and there was a great influence of calculating the initial position on the original UC, namely UC-LD. The UC-LD method applies to the modified uniformity coefficient based on modified L_2-star discrepancies. A Koksma-Hlawka-type inequality is applicable to uniformity coefficient based on wrap-around discrepancy (UC-WD) as well as uniformity coefficient based on centred discrepancy(UC-CD) theoretically. In addition, they show some advantages includ-

ing rotation invariance (reflection invariance), permutation invariance and the ability to measure projection uniformity. Analysing real experimental cases and simulating to evaluate the performance of the novel method. The experimental results show that UC-CD presents more sensitive performance than UC-WD so the UC-CD is more appropriate for industry.

In summary, we believe that on the basis of a large amount of previously published works, the complexity of the bubble swarm patterns can be reduced and their mechanisms clarified, and the heat transfer performance in a DCHE can be elucidated.

Acknowledgement

This work is supported by the National Natural Science Foundation of China (51666006, 51406071) and Scientific and Technological Leading Talent Projects in Yunnan Province (2015HA019).

Author details

Hua Wang*, Qingtai Xiao and Jianxin Xu

*Address all correspondence to: wanghua65@163.com

Kunming University of Science and Technology, Kunming, PR China

References

[1] S. Kar, X.D. Chen, M.I. Nelson, Direct-contact heat transfer coefficient for condensing vapour bubble in stagnant liquid pool, Chem. Eng. Res. Des. 85 (3) (2007) 320–328.

[2] C.P. Ribeiro Jr., P.L.C. Lage, Population balance modeling of bubble size distributions in a direct-contact evaporator using a sparger model, Chem. Eng. Sci. 59 (12) (2004) 2363–2377.

[3] T. Lemenand, C. Durandal, D. Della Valle, H. Peerhossaini, Turbulent directcontact heat transfer between two immiscible fluids, Int. J. Therm. Sci. 49 (10) (2010) 1886–1898.

[4] T. Nomura, M. Tsubota, T. Oya, N. Okinaka, T. Akiyama, Heat storage in direct contact heat exchanger with phase change material, Appl. Therm. Eng. 50 (1) (2013) 26–34.

[5] H.B. Mahood, Direct-contact heat transfer of a single volatile liquid drop evaporation in an immiscible liquid, Desalination 222 (1–3) (2008) 656–665.

[6] Y.J. Hyun, J.H. Hyun, W.G. Chun, Y.H. Kang, An experimental investigation into the operation of a direct contact heat exchanger for solar exploitation, Int. Commun. Heat Mass Transfer 32 (3–4) (2005) 425–434.

[7] M.N.A. Hawlader, M.A. Wahed, Analyses of ice slurry formation using direct contact heat transfer, Appl. Energy 86 (7–8) (2009) 1170–1178.

[8] Nguyen D, Rasmuson A, Niklasson Bjorn I, Thalberg K. CFD simulation of transient particle mixing in a high shear mixer. Powder Technol 258 (2014) 324–330.

[9] S. Kim, A.N. Nkaya, T. Dyakowski, Measurement of mixing of two miscible liquids in a stirred vessel with electrical resistance tomography, Int. Commun. Heat Mass Transfer 33 (9) (2006) 1088–1095.

[10] T. Maruyama, S. Yoshida, T. Mizushina, The flow regime transition in a bubble column, J. Chem. Eng. Jpn. 14 (1981) 352–357.

[11] H.T. Bi, J.R. Grace, Regime transitions: analogy between gas-liquid cocurrent upward flow and gas-solid upward transport, Int. J. Multiphase Flow 22 (2000) 1–19.

[12] M.C. Ruzicka, J. Zahradnik, J. Drahos, N.H. Thomas, Homogeneous heterogeneous regime transition in bubble columns, Chem. Eng. Sci. 56 (15) (2001) 4609–4626.

[13] C.P. Ribeiro Jr., P.L.C. Lage, Direct-contact evaporation in the homogeneous and heterogeneous bubbling regimes. Part I: experimental analysis, Int. J. Heat Mass Transfer 47 (17–18) (2004) 3825–3840.

[14] C.P. Ribeiro Jr., C.P. Borges, P.L.C. Lage, Sparger effects during the concentration of synthetic fruit juices by direct-contact evaporation, J. Food Eng. 79 (3) (2007) 979–988.

[15] A.-L. Le Coënt, A. Rivoire, S. Briancon, J. Lieto, An original image-processing technique for obtaining the mixing time: The box-counting with erosions method, Powder Technol. 152 (1–3) (2005) 62–71.

[16] S.M. Peyghambarzadeh, M.M. Sarafraz, N. Vaeli, E. Ameri, A. Vatani, M. Jamialahmadi, Forced convective and subcooled flow boiling heat transfer to pure water and n-heptane in an annular heat exchanger, Ann. Nucl. Energy 53 (0) (2013) 401–410.

[17] J.M. Hyde, M.K. Miller, M.G. Hetherington, A. Cerezo, G.D.W. Smith, C.M. Elliott, Spinodal decomposition in Fe-Cr alloys: experimental study at the atomic level and comparison with computer models III. Development of morphology, Acta Metall. Mater. 43 (9) (1995) 3415–3426.

[18] M. Gameiro, K. Mischaikow, T. Wanner, Evolution of pattern complexity in the Cahn-Hilliard theory of phase separation, Acta Mater. 53 (2005) 693–704.

[19] J.M. Friedrich, Quantitative methods for three-dimensional comparison and petrographic description of chondrites, Comput. Geosci. 34 (12) (2008) 1926–1935.

[20] S.S. Gulawani, S.K. Dahikar, C.S. Mathpati, J.B. Joshi, M.S. Shah, C.S. RamaPrasad, D.S. Shukla, Analysis of flow pattern and heat transfer in direct contact condensation, Chem. Eng. Sci. 64 (8) (2009) 1719–1738.

[21] S.S. Gulawani, J.B. Joshi, M.S. Shah, C.S. RamaPrasad, D.S. Shukla, CFD analysis of flow pattern and heat transfer in direct contact steam condensation, Chem. Eng. Sci. 61 (16) (2006) 5204–5220.

[22] S.K. Dahikar, M.J. Sathe, J.B. Joshi, Investigation of flow and temperature patterns in direct contact condensation using PIV, PLIF and CFD, Chem. Eng. Sci. 65 (16) (2010) 4606–4620.

[23] A.B. Tayler, D.J. Holland, A.J. Sederman, L.F. Gladden, Exploring the origins of turbulence in multiphase flow using compressed sensing MRI, Phys. Rev. Lett. 108 (26) (2012) 1–5. 264504.

[24] Q. Zhang, Y. Yong, Z.S. Mao, C. Yang, C. Zhao, Experimental determination and numerical simulation of mixing time in a gas–liquid stirred tank, Chem. Eng. Sci. 64 (12) (2009) 2926–2933.

[25] A. Zhang, V.L. Tsang, R. Korke-Kshirsagar, T. Ryll, Effects of pH probe lag on bioreactor mixing time estimation, Process Biochem. 49 (6) (2014) 913–916.

[26] Y. Zhao, X. Li, J. Cheng, C. Yang, Z.S. Mao, Experimental study on liquid–liquid macromixing in a stirred tank, Chem. Eng. Sci. 50 (10) (2011) 5952–5958.

[27] D.M. Fries, P.R.V. Rohr, Liquid mixing in gas–liquid two-phase flow by meandering microchannels, Chem. Eng. Sci. 64 (6) (2009) 1326–1335.

[28] D. Nguyen, A. Rasmuson, I.N. Björn, K. Thalberg, Cfd simulation of transient particle mixing in a high shear mixer, Powder Technol. 258 (258) (2014) 324–330.

[29] S.L. Yeoh, G. Papadakis, M. Yianneskis, Determination of mixing time and degree of homogeneity in stirred vessels with large eddy simulation, Chem. Eng. Sci. 60 (s 8–9) (2005) 2293–2302.

[30] J. Behin, N. Farhadian, Residence time distribution measurements in a two dimensional rectangular airlift reactor by digital image processing, Exp. Thermal Fluid Sci. 51 (11) (2013) 244–250.

[31] F. Cabaret, S. Bonnot, L. Fradette, P.A. Tanguy, Mixing time analysis using colorimetric methods and image processing, Ind. Eng. Chem. Res. 46 (14) (2007) 5032–5042.

[32] J. Huang, J. Xu, X. Sang, H. Wang, W. Hua, Quantifying the synergy of bubble swarm patterns and heat transfer performance using computational homology, Int. J. Heat Mass Transf. 75 (4) (2014) 497–503.

[33] G. Rodriguez, T. Anderlei, M. Micheletti, M. Yianneskis, A. Ducci, On the measurement and scaling of mixing time in orbitally shaken bioreactors, Biochem. Eng. J. 82 (3) (2014) 10–21.

[34] W.H. Woodall, Controversies and contradictions in statistical process control, J. Qual. Technol. 1 (4) (2000) 341–350.

[35] M. Panda, P.M. Khilar, Distributed self fault diagnosis algorithm for large scale wireless sensor networks using modified three sigma edit test, Ad Hoc Netw. 25 (2015) 170–184.

[36] Xu J, Xiao Q, Fei Y, et al. Accurate estimation of mixing time in a direct contact boiling heat transfer process using statistical methods, Int. Commun. Heat Mass Transf. 75 (2016) 162–168.

[37] Fang KT, Wang Y. Number theoretic methods in statistics. Chapman & Hall CRC Press London, UK: 1994.

[38] Fang KT. Uniform design application of number theory to experimental design. Acta Math Appl Sin 3 (1980) 363e72.

[39] Xu J, Xiao Q, Chen Y, et al. A modified L_2-star discrepancy method for measuring mixing uniformity in a direct contact heat exchanger,Int. J. Heat Mass Transf. 97 (2016) 70–76.

[40] Y. Fei, Q.-T. Xiao, J.-X. Xu, J.-X. Pan, S.-B. Wang, H. Wang, J.-W. Huang, A novel approach for measuring bubbles uniformity and mixing efficiency in a direct contact heat exchanger, Energy 93 (2) (2015) 2313–2320.

[41] S. Heinrich, Efficient algorithms for computing the -discrepancy, Math. Comput. Am. Math. Soc. 65 (216) (1996) 1621–1633.

[42] F. Hickernell, A generalized discrepancy and quadrature error bound, Math. Comput. Am. Math. Soc. 67 (221) (1998) 299–322.

[43] S. Thongwik, N. Vorayos, T. Kiatsiriroat, A. Nuntaphan, Thermal analysis of slurry ice production system using direct contact heat transfer of carbon dioxide and water mixture, Int. Commun. Heat Mass Transfer 35 (6) (2008) 756–761.

[44] T. Kaczynski, K. Mischaikow, M. Mrozek, Computational Homology, SpringerVerlag, New York, 2004.

[45] CHomP. http://chomp.rutgers.edu/software.

[46] N.W. Smirnow, I.W. Dunin-Barkowski, Mathematische statistik in der technik, Veb Deutscher Verlag Der Wissenschaften, Berlin, 1969.

[47] J. Xu, H. Wang, H. Fang, Multiphase mixing quantification by computational homology and imaging analysis, Appl. Math. Modell. 35 (5) (2011) 2160–2171.

[48] Niederreiter H. Random number generation and quasi-Monte Carlo methods. Philadelphia: SIAM; 1992. MR 93h 62135.

[49] T.T. Warnock, Computational investigations of low-discrepancy pointsets, in: S.K. Zaremba (Ed.), Applications of Number Theory to Numerical Analysis, Academic Press, New York, 1972, pp. 319–343.

[50] K.-T. Fang, R. Li, A. Sudjianto, Design and Modeling for Computer Experiments, CRC Press, Boca Raton, 2005.